

Time-Series Prediction Approaches to Forecasting Deformation in Sentinel-1 InSAR Data

P. Hill ¹, J. Biggs ², V. Ponce-López ¹, D. Bull ¹,

¹Department of Electrical and Electronic Engineering, University of Bristol, Bristol, United Kingdom
²COMET, School of Earth Sciences, University of Bristol, Bristol, United Kingdom

Key Points:

- We test established time series prediction methods on 4 years of Sentinel-1 InSAR data, and investigate the role of seasonality
- For seasonal signals, SARIMA and machine learning (LSTM) perform best over <3 months, and sinusoid extrapolation over >6 months.
- Forecast quality decreases for less seasonal signals, and a constant value prediction performs best for randomly-selected datapoints.

Corresponding author: Paul Hill, Paul.Hill@Bristol.ac.uk

Abstract

Time series of displacement are now routinely available from satellite InSAR and are used for flagging anomalous ground motion, but not yet for forecasting. Here we test the capabilities of conventional time series analysis and forecasting methods such as SARIMA and supervised machine learning approaches such as Long Short Term Memory (LSTM) in comparison to simple function extrapolation methods. For our initial tests, we focus on forecasting periodic signals and begin by characterising the time-series using sinusoid fitting, seasonal decomposition and autocorrelation functions. We find that the three measures are broadly comparable but identify different types of seasonal characteristic. We use this to select a set of 310 points with highly seasonal characteristics and test the three chosen forecasting methods over prediction windows of 1-9 months. The lowest overall RMSE values are obtained for SARIMA when considering short term predictions (<1 month), whereas sinusoid extrapolation performs best for longer predictions (>6 months). Machine learning methods (LSTM) perform less well, as is often the case for non-stationary signals. We then test the prediction methods on 2000 randomly selected points with a range of seasonalities and find that simple extrapolation of a constant function performed better overall than any of the more sophisticated time series prediction methods. Comparisons between seasonality and RMSE show a statistically significant improvement in performance with increasing seasonality. This proof-of-concept study demonstrates the potential of time-series prediction for InSAR data but also highlights the limitations of applying these techniques to non-periodic signals or individual measurements points. We anticipate future developments, especially to shorter timescales, will have a broad range of potential applications, from infrastructure stability to volcanic eruptions.

1 Introduction

Many tectonically stable regions suffer from significant ground motion due to the effects of former coalfields (McCay et al., 2018), landslides (Chambers et al., 2008), the shrink and swell of shallow clays (Crilly, 2001; Aldiss et al., 2014), tree growth, coastal erosion, natural sinkholes (Lamont-Black et al., 2002; Banks et al., 1995) and tunnelling (e.g. Cross-rail, (Milillo et al., 2018)). Ground motion analysis has recently focused on satellite-based InSAR, which uses the phase difference between pairs of radar satellite images to map ground deformation at mm/yr precision. In particular, the Copernicus Sentinel-1 constellation has revolutionised the coverage, frequency and availability of InSAR data and can be used to produce high resolution maps of ground motion across Europe every six days in near real-time. To this end, many companies have generated post-processed ground motion data maps and time series based on Sentinel-1 InSAR data (e.g. *cgg.com*; *satsense.com*; *tre-altamira.com*). Machine learning methods have been used to automatically flag deformation, or changes in deformation in the large datasets (Anantrasirichai et al., 2018, 2019a, 2019b; Gaddes et al., 2019; Valade et al., 2019). Here we investigate the possibility that these Sentinel-1 datasets can be used to forecast future behaviour.

Time series forecasting defines a prediction model to forecast future values of a univariate or multivariate time series based on previously observed values. Time series forecasting plays a significant role in many application domains such as econometrics, mathematical finance, electroencephalography, astronomy and communications engineering. Due to the financial importance of large scale forecasting of commodity values, time series forecasting has been led by disciplines associated with economics. Economic time series forecasting has led to standard time series prediction tools such as SARIMA (Box et al., 2015; Hamilton, 1994; Brockwell & Davis, 2016); a key forecasting tool evaluated within our work. More recently, Recurrent Neural Networks have been effectively used for time series prediction using methods such as LSTMs (Hochreiter & Schmidhuber, 1997; Greff et al., 2017) and sequence to sequence (Seq2Seq) methods (Sutskever et al., 2014; Cho et al., 2014). LSTM and Seq2Seq methods are easily adapted to both univariate or multivariate time series prediction (Rebane et al., 2018; Torres & Qiu, 2018).

65 For many of the processes that contribute to InSAR measurements, we expect that
 66 prior observations will not contain sufficient information to accurately predict future ob-
 67 servations. This includes both signals of interest, such as sudden catastrophic failures,
 68 and noise terms, such as turbulent atmospheric effects. However, some components of
 69 the signal have repeating characteristics, such as multi-year trends and seasonal effects.
 70 We begin by analysing the characteristics of the input dataset to select signals with re-
 71 peating characteristics with a period of 1 year (section 3), and then focus on forecast-
 72 ing over time periods of 1-9 months (section 4 and 5). Finally, we discuss the potential
 73 applications and current limitations of time-series forecasting for Sentinel-1 InSAR data.

74 2 Case Study Dataset

75 2.1 InSAR Data

76 We test our algorithms on Sentinel-1 data processed by Satsense Ltd using an algorithm
 77 based on the RapidSAR approach (Spaans & Hooper, 2016) (Figure 17). Atmospheric
 78 effects are the dominant source of noise in most InSAR datasets and have been reduced
 79 within the Satsense data through: (1) The removal of long wavelength signals from each
 80 InSAR image using a Gaussian spatial filter. (2) The removal of short wavelength at-
 81 mospheric signals using an APS (Atmospheric Phase Screen) filter. This isolates the random-
 82 in-time effects using a highpass filter and then uses a low-pass spatial filter to estimate
 83 the spatially correlated temporally random atmospheric effects. (3) Smoothing the dis-
 84 placemens in time using a per-time-series temporal filter to reduce the effects of over-
 85 all temporal noise which may include some residual atmospheric noise not removed by
 86 the APS filter.

87 Sentinel-1 acquires data every 6 days over Europe, but due to operational factors,
 88 some of this data is missing, particularly in the first year when only Sentinel-1A was op-
 89 erating. Since the algorithms proposed here require regularly sampled data, we interpo-
 90 late onto an even 6-day temporal grid as shown in Supplementary Figure 1. Simple lin-
 91 ear interpolation between neighbours is used to avoid unnecessary assumptions.

92 2.2 Case Study Area

93 This project is part of the UK Digital Environment Programme and we use the subsi-
 94 dence of the West Yorkshire coal mines as a case study (Burke et al., 2015; Lake et al.,
 95 1992). Here we choose to work on the area around Normanton, which was mined until
 96 the mid-1970s and where there is a high density of InSAR scatterers (Figure 1). The area
 97 is currently subsiding at a rate of up to 15mm/yr and superimposed on this are seasonal
 98 signals, particularly associated with some of the large warehouse buildings in the area.

99 A subset of the time series (points P1-P8) have been selected for further analysis
 100 and forecasting experiments, and these are shown in Figure 1. P1-P3 illustrate the com-
 101 bination of a (downward) trend and seasonality; P4-P6 have a strong seasonal signal, but
 102 no long-term trend, and P7 and P8 show trends without seasonality. Points P1-P6 were
 103 selected as being the top six seasonal signals according to the analysis in section 3 and
 104 points P7 and P8 the lowest. P1-P3 and P6-P7 are car parks; P4 and P5 are the roofs
 105 of a house and P8 is the roof of the XPO Logistics warehouse.

106 3 Seasonal Signals in the InSAR Dataset

107 3.1 Measures of Seasonality

108 Our hypothesis is that InSAR signals contain some periodic components, for which time
 109 series forecasting may be useful. For this application, we chose to focus on the most com-
 110 mon natural periodic variations, those that occur annually. We start by testing the most

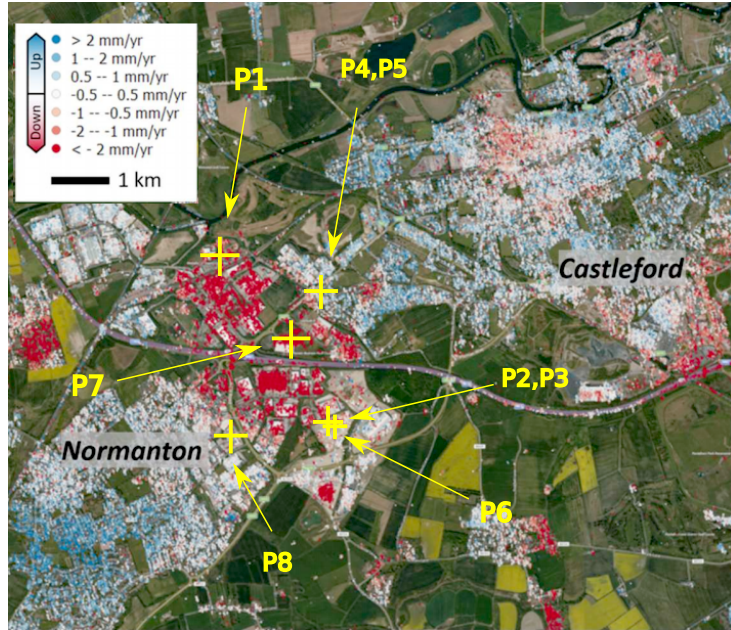


Figure 1. Large scale subsidence in West Yorkshire due to historical shallow coal mining. Central figure shows colour coded motion magnitudes. Points P1-P8 show the chosen points for analysis. P1-P3 illustrate the combination of a (downward) trend and seasonality; P4-P6 have a strong seasonal signal, but no long-term trend, and P7 and P8 show trends without seasonality. P1-P3 and P6-P7 are car parks; P4 and P5 are the roofs of a house and P8 is the roof of the XPO Logistics warehouse. Corresponding time series are shown in Figure 8

111 commonly used method for estimating and removing seasonal components of geodetic
 112 timeseries, namely sinusoid fitting (Watson et al., 2002; Colesanti et al., 2003). However,
 113 this measures the correlation with purely sinusoidal behaviour and could potentially ex-
 114 clude periodic signals with other non sinusoidal but repeating waveforms. First, we re-
 115 view a variety of methods of detecting seasonality (Hartmann et al., 1992; Zubaidi et al.,
 116 2018; Hylleberg, 1995) and summarise them in Supp. Table 1. We then focus on meth-
 117 ods that are able to generate quantitative measures of annual seasonality rather than sim-
 118 ple detection and can be used to analyse pre-defined periods (12 months) rather than
 119 estimate the period of seasonality. Based on these criteria, we select 'Seasonal and Trend
 120 decomposition using Loess' (STL)(R. B. Cleveland et al., 1990) and autocorrelation func-
 121 tion (ACF)(Chen & Boccelli, 2018) for further study. The choice of whether or not to
 122 normalise the seasonality measures is a key design decision. With normalisation the am-
 123 plitude of the seasonality will be disregarded, but if there is no normalisation, high am-
 124 plitude stochastic signal components will often mask truly seasonal signals with small
 125 amplitude. For this reason, all three considered seasonality measures are normalised.

126 **3.1.1 Sinusoid Fitting and Correlation (Sin) Method**

127 We fit a sinusoid of fixed frequency (12 months) to the detrended time series using a least
 128 squares method and extract the amplitude and phase parameters. An obvious measure
 129 of seasonality is the magnitude of the fitted sinusoid, however, in this case, large mag-
 130 nitude signals that are not particularly seasonal will produce a bigger seasonality index
 131 than smaller magnitude signals that are truly seasonal. Instead, we define the seasonal

132 index for this method to be the normalised correlation between the training signal and
 133 the fitted sinusoid,

$$\text{SIndex}_{\text{Sin}} = \rho(W_t, \hat{W}_{\text{sin}}) \quad (1)$$

134 where ρ is normalised correlation and \hat{W}_{sin} is the fitted sinusoid.

135 3.1.2 STL decomposition

136 The concept of a “seasonal decomposition” of a time series signal means that the time
 137 series can be decomposed into a sum (or a product) of three components: a trend, a sea-
 138 sonal component, and a residual. We have used the common implementation of STL as
 139 initially described by Cleveland (R. B. Cleveland et al., 1990) assuming an additive STL
 140 model. This implementation uses Loess smoothing, which uses iterative sliding window
 141 regression to generate smooth functions (seasonal and trend) (W. S. Cleveland, 1979).
 142 First Loess smoothing is applied to remove the seasonal component then a separate Loess
 143 smoothing is applied to remove the trend. The remaining component is the residual.

144 A logical measure of the seasonality can then be defined using the ratio of the vari-
 145 ance of the residual (L) to the variance of the signal without the trend (L+S). As this
 146 ratio increases as seasonality decreases, we define seasonality as follows. $\text{SIndex}_{\text{STL}}$ is
 147 mathematically well behaved and varies from 0 to 1.

$$\text{SIndex}_{\text{STL}} = 1.0 - \frac{\text{Var}[L]}{\text{Var}[L + S]} \quad (2)$$

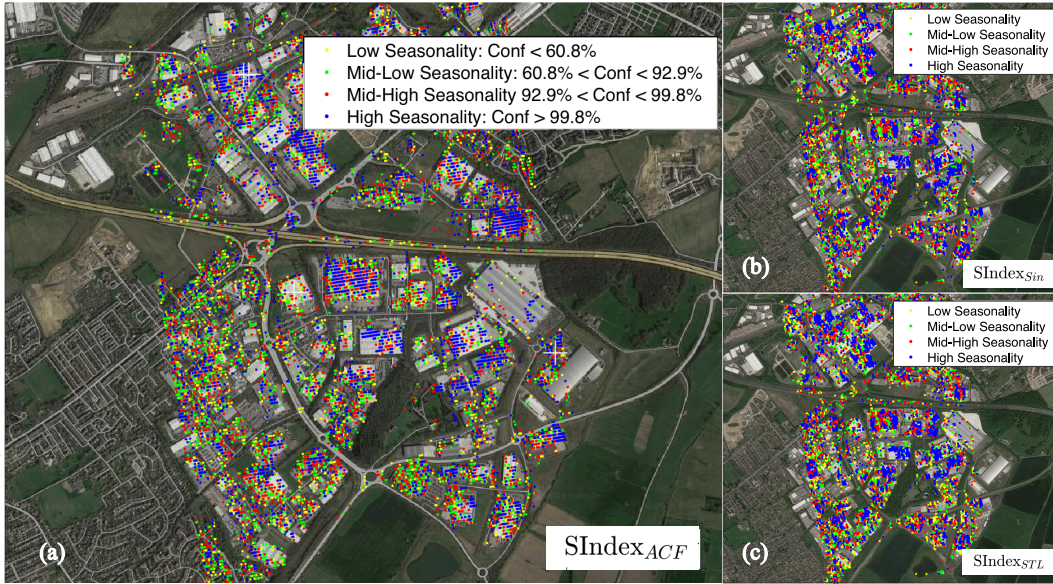


Figure 2. Dataframe of InSAR datapoints in Normanton area grouped by levels of seasonality using; (left) $\text{SIndex}_{\text{ACF}}$, (top right) $\text{SIndex}_{\text{STL}}$, and (bottom right) $\text{SIndex}_{\text{Sin}}$. The $\text{SIndex}_{\text{ACF}}$ sub figure is divided into four ranges of confidence bounds. Confidence is calculated as the rejection of the Null hypothesis that the ACF value is insignificant using the standard errors under the assumption of a Gaussian source (as used by the MATLAB `autocorr` function). Seasonality indices $\text{SIndex}_{\text{STL}}$ and $\text{SIndex}_{\text{Sin}}$ are divided into four equal and sorted ranges of seasonality indexed by colour.

148

3.1.3 Autocorrelation Function (ACF) Method

149

150

151

152

153

154

155

The autocorrelation function (ACF) measures how self-similar a signal is by measuring the correlation of the signal with shifted versions of itself (Chen & Boccelli, 2018; Carla et al., 2016). These shifts are known as lags and in this case, we are only interested in the lag corresponding to 12 months. As the InSAR signal is sampled every 6 days (from 2015 to 2018) the lag is set to be 60. $SIndex_{ACF}$ is well behaved and varies from 1 (perfect correlation) to -1 (perfect anti-correlation). It is defined in (3) where ρ is the normalised ACF function (with lag 60).

$$SIndex_{ACF} = \rho_{60}(W_t) \quad (3)$$

156

157

158

159

160

161

162

In order to properly estimate seasonality, isolated from the influence of trend, the trend is removed by fitting a second degree polynomial to the InSAR time series and subtracting it when using the ACF method. A second-degree polynomial was chosen to properly model DC variations over the trained signal (this is not done for the STL method where the trend is extracted independently). Confidence values can then be calculated as the rejection of the null hypothesis that the ACF value is insignificant using standard errors under the assumption of a Gaussian source.

163

3.1.4 Comparison of seasonality measures

164

165

166

167

168

For the ACF method (Figure 2(a)), seasonality correlates well with land use type, with the highest values attributed to the roofs of particular buildings (for example the Wakefield ASDA distribution centre). Figures 2(b) and 2(c) show that sinusoid fitting and STL methods are less spatially correlated (in terms of the different seasonality magnitudes) when compared to the ACF based measure.

169

170

171

172

173

174

175

176

Figure 3 shows a comparison of the seasonality measures $SIndex_{Sin}$, $SIndex_{STL}$ and $SIndex_{ACF}$ for all the datapoints in Normanton region (with points P1-8 labelled). The approximately linear relationship between the measures demonstrates that they are broadly comparable, and the points P1-6 are classified as highly seasonal by all three indices, whereas P7-8 lie with the majority of points which are not seasonal. However, there is considerable scatter showing that the three indices identify different types of seasonality, with especially large differences between the ACF and STL measures. We use the ACF measure for the subsequent experiments.

177

4 Ground Motion Forecasting

178

179

180

181

182

183

184

The task of forecasting InSAR time series can be approached in one of three ways: 1) Future displacements forecast on each point individually, using only information from that point (Mazzanti et al., n.d.); 2) Future displacements can be forecast for each point individually, using the time series itself and a selected group of related time series; 3) Groups of time series can be forecast in a multidimensional sense (Rebane et al., 2018; Torres & Qiu, 2018). For this proof-of-concept, we have focused on the first two approaches for simplicity.

185

186

187

188

189

190

191

192

193

In this paper, we evaluate the forecasting methods by dividing each signal into a “training” sub-range and a contiguous “testing” sub-range in order to be able to generate objective evaluations of each forecast. That is, given an entire temporal signal of T datapoints $W = \{w_1, w_2, \dots, w_T\}$, we define “today” as being timestep = t and our goal is to predict a new signal $\hat{y} = \{\hat{w}_{t+1}, \hat{w}_{t+2}, \dots, \hat{w}_{t+N_y}\}$ as similar as possible to the original sub-signal $y = \{w_{t+1}, w_{t+2}, \dots, w_{t+N_y}\} \in W$. We also define the training set as $W_t = \{w_1, w_2, \dots, w_t\} \in W$. The value N_y is a positive scalar integer which determines the period of time to be forecast - i.e. the number of future observations. We set N_y to approximately 9 months (264 days) for all experiments, but evaluate the predic-

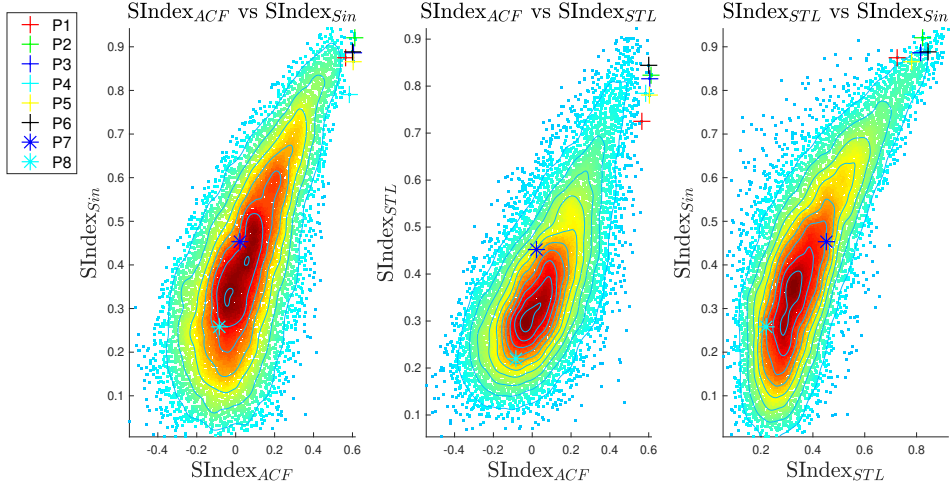


Figure 3. Comparison of Seasonality Measures $SIndex_{Sin}$ is the normalised correlation between the signal and the best-fitting sinusoid. $SIndex_{STL}$ is based on a seasonal decomposition (STL) and defined as defined using the ratio of the variance of the residual (L) to the variance of the signal without the trend (L+S). $SIndex_{ACF}$ is the normalised autocorrelation function with a period of 1 year (or 60 datapoints)

194 tion over time periods of 1-9 months. The value N_x is a positive scalar integer which de-
 195 termines the period of time for training i.e. the number of past observations. An illus-
 196 trative example of the predicted and test signals is shown on the right of Figure 4.

197 A summary of all the forecast methods compared is given in Table 1. In order to
 198 compare the SARIMA and LSTM approaches with previously used methods, we include
 199 a standard sinusoid fitting algorithm (Watson et al., 2002), and project the fit forward
 200 in time. A sinusoid and trend are fitted to the same part of the each of the time series
 201 as used for training the other methods (i.e. W_t) and future values extrapolated using the
 202 resulting parameterisation.

203 4.1 Long Short-Term Memory (LSTM) Networks

204 A Long Short-Term Memory (LSTM) (Hochreiter & Schmidhuber, 1997; Greff et al., 2017)
 205 network is a Recurrent Neural Network (RNN) (Rumelhart et al., 1986) architecture used
 206 in the field of deep learning for time series data. RNNs keep track of arbitrary long-term
 207 dependencies in the input sequences, and they can scale to much longer sequences than
 208 classical networks. They are designed to process sequences of variable lengths, where pa-
 209 rameters are shared with all previous output members. LSTMs have the ability to add
 210 or remove information to a temporal learning "state". This is carefully regulated by struc-
 211 tures called gates. The learning selectively *keeps* some part of the past (using the tem-
 212 poral states) and *forgets* others (using "forget" gates). LSTMs are commonly used for
 213 classification applications. However, within this application we are using them within
 214 the regression framework illustrated in Figure 4 where the output of the network \hat{y} is an
 215 array of length N_y .

Table 1. Summary of Forecasting Methods. For all methods $N_x = 9$ months, $N_y = 9$ months

Method	Definition
Constant	A constant value prediction, taking the last value of the training time series and extrapolating it for the whole of the test series.
Sinu	Sinusoid fitting method: A simplex gradient descent method was used to fit the amplitude and phase of a sinusoid to the data (together with the slope of a linear trend term).
SARIMA	SARIMA based prediction with parameters obtained using the “auto sarima” method (Hyndman et al., 2007).
LSTM1	Single signal used for prediction (based on the univariate method illustrated in Figure 4). Architecture included: two LSTM layers (first with 256 nodes and second with 128 nodes). The final state output of the second LSTM layer is connected to a dense layer of 128 nodes and then subsequently connected to an output layer with N_y nodes. Dropout of level 0.5 is included between each layer, the activation function was ReLU, the loss was MSE, the optimiser was ADAM.
LSTM2	The six most seasonal signals (seasonality measured using $SINDEX_{ACF}$) concatenated and used for training (Figure 5). The remaining architectural features for this as per LSTM1.
LSTM3	The top 1% of the seasonal signals (seasonality measured using $SINDEX_{ACF}$) concatenated and used for training as per LSTM2.
LSTM4	The eight spatially closest time series signals (see Supp. Figure 1b) are formed into different features in the multivariate learning process (with a single dimensional feature predicted for the considered time series).
Seq2Seq1	Seq2Seq architecture. The encoder was a single encoder LSTM layer (with 200 nodes) whose output was copied N_y times. This time distributed output was then input into the decoder; a single LSTM layer (with 200 nodes). This was then input to a fully connected dense layer with a final single (but time distributed output layer) node. No dropout was used. The remaining aspects of this architecture were as per LSTM1.
Seq2Seq2	Same as LSTM2 but with Seq2Seq architecture as described for Seq2Seq1.
Seq2Seq3	Same as LSTM3 but with Seq2Seq architecture as described for Seq2Seq1..
Seq2Seq4	Same as LSTM4 but with Seq2Seq architecture as described for Seq2Seq1.

216

4.1.1 Univariate LSTM: LSTM1

217

218

219

220

221

222

223

224

225

226

Figure 4 shows the univariate case of forecasting ground motion using a supervised LSTM network. A sliding window forms a training data frame (for a single signal) of inputs (\mathbf{X}) and outputs (\mathbf{Y}) to train the network. Once trained, the testing input (\mathbf{X}_{test}) is ingested into the network to generate the forecast \hat{y} approximating the true sequence y . This requires a final layer in the network to generate a vector the same length as y . This is done using a fully connected dense layer without any subsequent pooling as illustrated in Figure 5. For all the subsequent experiments N_x and N_y are set to 9 months (264 days). This was considered to be long enough to characterise the seasonal nature of the signals, be able quickly to adapt to changes and also have the maximum amount of training data from the sliding window. We use a network of two LSTM layers fully connected to a dense

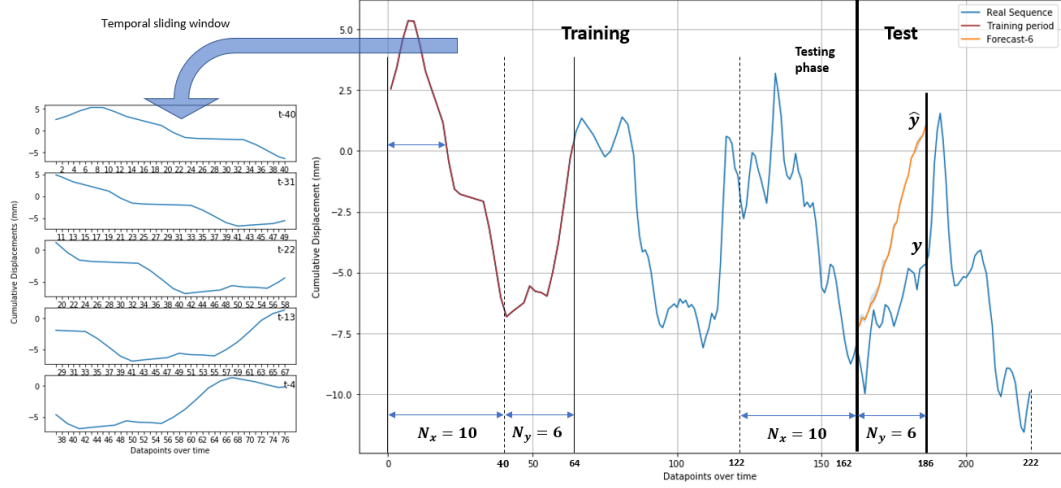


Figure 4. Example of a multi-step approach for time-series forecasting. The considered signal is split into training and test sets. The training set contains the observable data and the test signal \mathbf{y} represents the future observations in the test set. This test signal is to be compared with the predicted signal $\hat{\mathbf{y}}$ obtained by our method as well as its associated prediction error. Our multi-step approach for LSTMs reframes the whole training data into temporal sliding windows of sizes N_x and N_y for past and future observations, respectively.

227 layer outputting the N_y regression outputs. Each layer has an integrated dropout func-
 228 tion (set to a dropout factor of 0.5 to prevent overfitting). The optimisation was based
 229 on the ADAM method (Kingma & Ba, 2015) and Mean Square Error (MSE) as the loss
 230 function. We train our networks using 2000 iterations (epochs) to achieve convergence.

231 4.1.2 Multi-Signal LSTM: LSTM2-4

232 We adapt the univariate approach shown in Figure 4 to include data from a set of training
 233 signals. This multi-signal LSTM is illustrated in Figure 5. This system uses the same
 234 network structure as above but vertically concatenates all of the sliding window data from
 235 a set of training signals. The testing data remains the same. The LSTM2 system uses
 236 the top six seasonal signals for training. The LSTM3 system uses the top 1% of the sea-
 237 sonal signals (using the $SINDEX_{ACF}$ method) for training. Conversely, LSTM4 uses the
 238 eight spatially closest time series signals as features in an eight-dimensional multivariate
 239 LSTM input. A multivariate LSTM architecture is then used to generate a univariate
 240 forecast from the multivariate InSAR derived ground motion time series data.

241 4.1.3 Seq2Seq LSTMs: Seq2Seq1-4

242 Sequence to sequence (Seq2Seq) is an encoder-decoder deep learning architecture for mak-
 243 ing multi-step predictions (Sutskever et al., 2014; Cho et al., 2014). The previous meth-
 244 ods (LSTM1-4) generated the prediction vector using the single output of an LSTM layer
 245 together with dense and fully connected layers (with a final vector regression output).
 246 Seq2Seq methods have an independent encoder that analyses the input time sequence
 247 and generates a characterising set of states that are subsequently input into the decoder.
 248 We have used a single LSTM layer as the encoder that outputs the LSTM states of the
 249 input time series data as an initial stage. These output states are then copied multiple
 250 times (with the number of copies being the required length of the prediction vector out-
 251 put). These copies then form a multidimensional time series input to a decoder (another

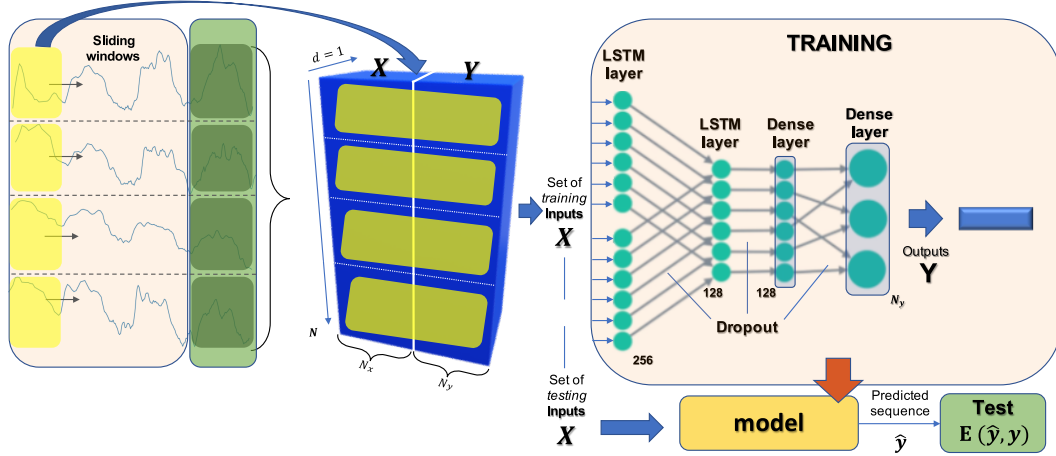


Figure 5. Multi-Signal LSTM. Every signal in the training set is split into training and test sets in the multi-signal approach. First, we use the training sets to frame every signal as a supervised machine learning problem, constructed by a set of inputs \mathbf{X} and outputs \mathbf{Y} . Each considered time-step for the sliding window for each signal becomes a sample in the feature space of input \mathbf{X} and output \mathbf{Y} of the network.

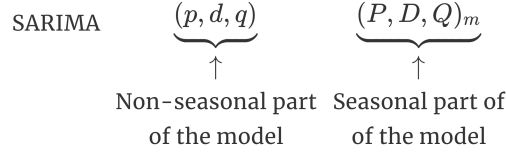
252 single LSTM layer). The time distributed outputs are then input into time distributed
 253 dense layers outputting a vector forecast result \hat{y} . Each method LSTM1-4 has been mod-
 254 ified to include a Seq2Seq architecture to form methods Seq2Seq1-4 respectively i.e. the
 255 other architectural forms and input/output data structures are equivalent for these two
 256 sets of methods.

257 4.2 SARIMA

258 SARIMA is an analysis and prediction method for time series data (Box et al., 2015; Hamil-
 259 ton, 1994; Brockwell & Davis, 2016). It is used to model non-stationary data series, where
 260 the data are not statistically consistent across time e.g. mean and variance varies with
 261 time. It is an analysis tool primarily used to model economic data and is able to iden-
 262 tify, model and predict both trend and seasonality (and their variations) over time. SARIMA
 263 consists of two sets of forecasting models: trend and seasonality. Each of these two mod-
 264 els are divided into three submodels: an autoregressive model (AR) and a Moving Av-
 265 erage (MA) model in order to model time variations (“tendencies”). The MA model is
 266 the equivalent of an estimated Finite Impulse Response (FIR) filter that just weights re-
 267 cent inputs to combine into an estimated output. Conversely, the AR model is an esti-
 268 mated all-pole or Infinite Impulse Response Filter (IIR) that uses a feedback loop to es-
 269 timate output given a weighted sum of previous outputs. The input is often further lo-
 270 cally differenced (the I stage) to model changes in offset (the third submodel).

271 The model is comprised of these three sub-models (AR, MA and I) estimated di-
 272 rectly on the data to model trend but also over a set lag directly related to the season-
 273 ality of the signal. A SARIMA model is then defined as the order of these six models
 274 (plus the analysis seasonality lag m):

275 where p is the order of the AR term, q is the order of the MA term, d is the num-
 276 ber of differencing operations required to make the time series stationary, P is the or-
 277 der of the AR seasonality term, Q is the order of the MA seasonality term, D is the num-



278 ber of differencing operations required to make the seasonal time series stationary and
279 m is the seasonality lag.

280 The parameters of the SARIMA model are commonly not estimated automatically
281 i.e. the statistics and correlation of the time series signal is analysed by hand and the
282 parameters are tuned until the signal (when compensated by the found parameters) is
283 considered to be stationary. However, recent automatic parameter estimation methods
284 do a minimisation search on some training data to determine the best combination of
285 SARIMA parameters (Hyndman et al., 2007). This method estimates the stationarity
286 of the signal under the parameters and specifically uses the Akaike Information Crite-
287 rion (AIC) and the Bayesian Information Criterion (BIC) estimators to compare mod-
288 els. The lower these values, the better the model fits the data (Hyndman et al., 2007).

289 Here, SARIMA parameters are fitted to the training data using Hyndman’s method
290 (Hyndman et al., 2007). A typical model for the analysed InSAR time series below was
291 SARIMA(3, 0, 2)(1, 1, 0)₆₀. The parameters are estimated using the same part of each
292 of the time series as used for training with LSTMs (i.e. W_t) and then SARIMA is used
293 to predict the same part of each time series as with LSTMs (i.e. W_y).

294 5 Forecast Performance

295 5.1 Seasonal Signals

296 We test the forecasting performance of LSTMs and SARIMA on a set of 310 highly sea-
297 sonal signals selected using the SIndex_{ACF} metric. We benchmark the results against si-
298 nusoid extrapolation and a constant value prediction. To assess the performance of each
299 model, we use the Root Mean Square Error, $RMSE(\hat{\mathbf{y}}) = \sqrt{\mathbf{E}((\hat{\mathbf{y}} - \mathbf{y})^2)}$ (Figures 6, 7).
300 We also consider normalised RMSE and define n1RMSE and n2RMSE as the RMSE of
301 the prediction normalised against the variance and constant value prediction respectively
302 (Supp. Figures 2-5). The RMSE distributions are displayed in the form of a boxplot that
303 includes the quartiles of the distribution (the middle line in each box is the distribution
304 median).

305 For a one month prediction (Figure 6a), the best performing methods were SARIMA
306 and LSTM3, which performed marginally better than the constant value prediction. Of
307 the Seq2Seq methods, the best performers were the univariate version Seq2Seq1 and Seq2Seq4,
308 which was trained with using the 8 geographically closest points. For these short time
309 periods, the sinusoidal extrapolation method (Sinu) performed poorly, with a median RMSE
310 value considerably higher than that of the constant value prediction. Conversely, for longer
311 time periods (Figure 6b), the best performing method was sinusoid extrapolation, with
312 a median RMSE value about 75% of the constant value prediction. The best perform-
313 ing LSTMs were LSTM3 and LSTM4, while Seq2Seq1 and Seq2Seq4 continue to out-
314 perform the multi-signal Seq2Seq methods (Seq2Seq2-3). Over these time periods, most
315 of the methods outperformed the constant value prediction, with only LSTM2, Seq2Seq2
316 and Seq2Seq3 performing worse (when considering median value of n2RMSE: Supp. Fig-
317 ure 3).

318 For all the time periods considered, the multi-signal Seq2Seq models (Seq2Seq2-
319 3) trained using a set of seasonal signals performed worse than the univariate case (Seq2Seq1).

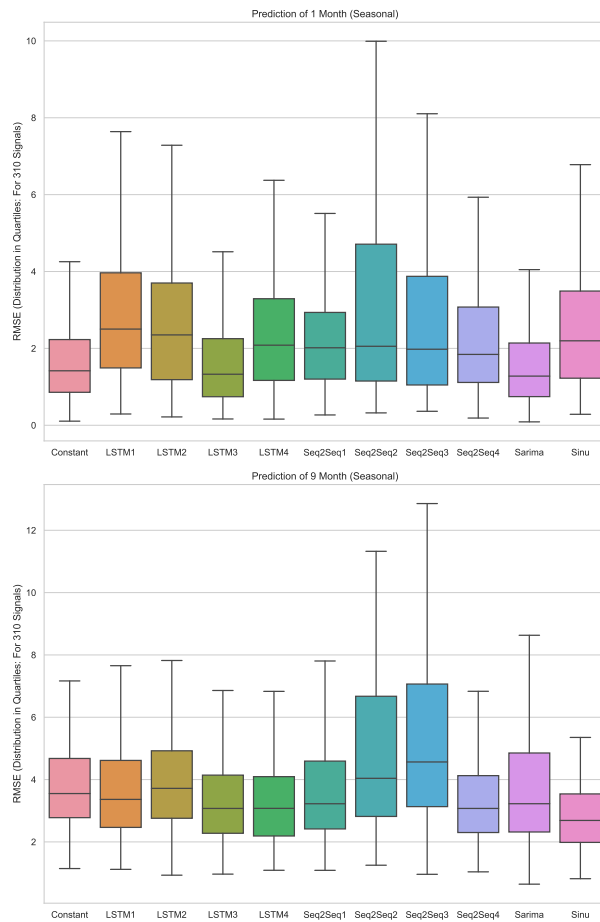


Figure 6. Forecast performance on seasonal signals. The boxplot lines represent the quartiles of the RMSE distribution for all 310 signals with coloured area being the central two quartiles and the central line being the median. a) performance over 1 month; b) performance over 9 months.

320 We conclude that any improvements gained by having a larger training dataset are off-
 321 set by the potentially unrelated data statistics and characteristics. However, Seq2Seq4,
 322 which was trained using geographically close signals, performed as well as, or a little bet-
 323 ter than, the univariate case (Seq2Seq1) suggesting that geographically close points have
 324 more similar signals, as for example, they may be located on the same structure.

325 Based on this assessment, we select LSTM3, Seq2Seq4 and SARIMA for further
 326 analysis and some examples of the predicted and real timeseries are shown in Figure 8.
 327 Points P1-P6 were selected as they have the most seasonal characteristics signals as de-
 328 fined by $SIndex_{ACF}$. All methods capture some aspects of the signal, and the timeseries
 329 plots are helpful in identifying sources of misfit. For example, sinusoid extrapolation is
 330 a global fitting method, so there is often a discontinuity between the training and pre-
 331 diction data (e.g. P3, P6; Figure 8), which explains why the RMSE is high when short
 332 prediction periods are considered (Figure 6a). Similarly, the SARIMA results can be
 333 seen to characterise the sub-seasonal variations of many of the example 6 signals, but
 334 for P1 and P2, the trend has not been accurately estimated and the prediction, although
 335 plausible in shape, has an inaccurate offset.

336 The results in Figure 6 suggests that performance varies according to prediction
 337 window, so we test the selected methods over periods of 1-9 months and compare the
 338 distribution of RSME values (Figure 7). The lowest RMSE values are obtained for SARIMA
 339 when considering short term predictions of < 3 months, whereas sinusoid extrapolation

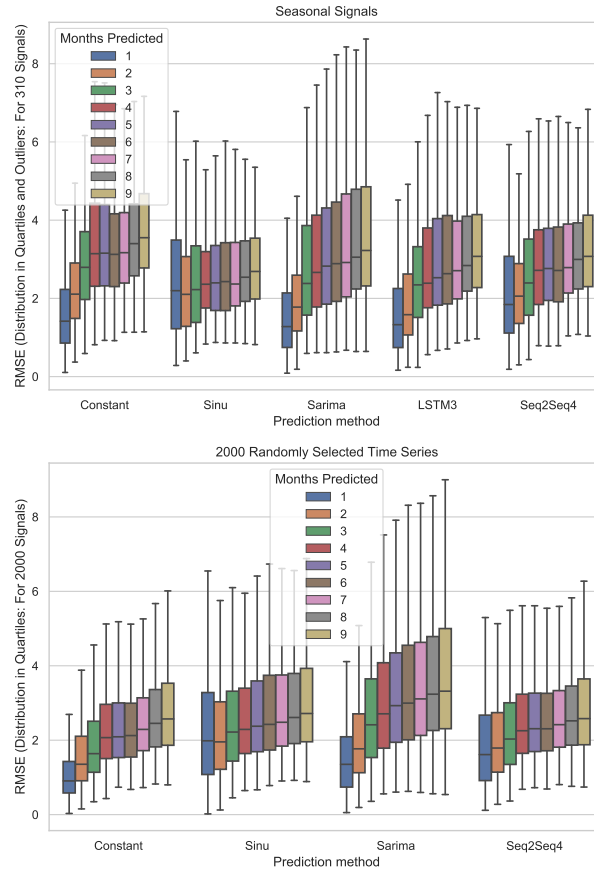


Figure 7. Forecast performance according to prediction window for a) 310 seasonal signals and b) 2000 randomly-selected signals. The boxplot lines represent the quartiles of the RMSE distribution with coloured area being the central two quartiles and the central line being the median.

340 performs best for predictions of > 6 months. As expected RMSE increases with increas-
 341 ing prediction window: the constant value prediction has a median RMSE value of 1.4
 342 cm for a 1 month window, increasing to 3.6 cm for a 9 month window. Normalising the
 343 RMSE to the RMSE value of the constant value prediction (n2RMSE, Supp. Figure 5)
 344 removes this effect, and shows that SARIMA and Seq2Seq4 outperform the constant value
 345 prediction for all windows, whereas Sinu and Seq2Seq4 only perform better when fore-
 346 casting 3 or more months into the future.

347 The multi-signal LSTM (LSTM3) gave the best results for short term prediction
 348 (< 3 months). SARIMA also gave good results for short term prediction but gave sig-
 349 nificantly worse results (compared to LSTM3) for predicting many months into the fu-
 350 ture. The performance of the Seq2Seq4 method was virtually identical to the LSTM3
 351 method for a period of 9 months but had a slightly larger median error (by 0.3cm) for
 352 1 month.

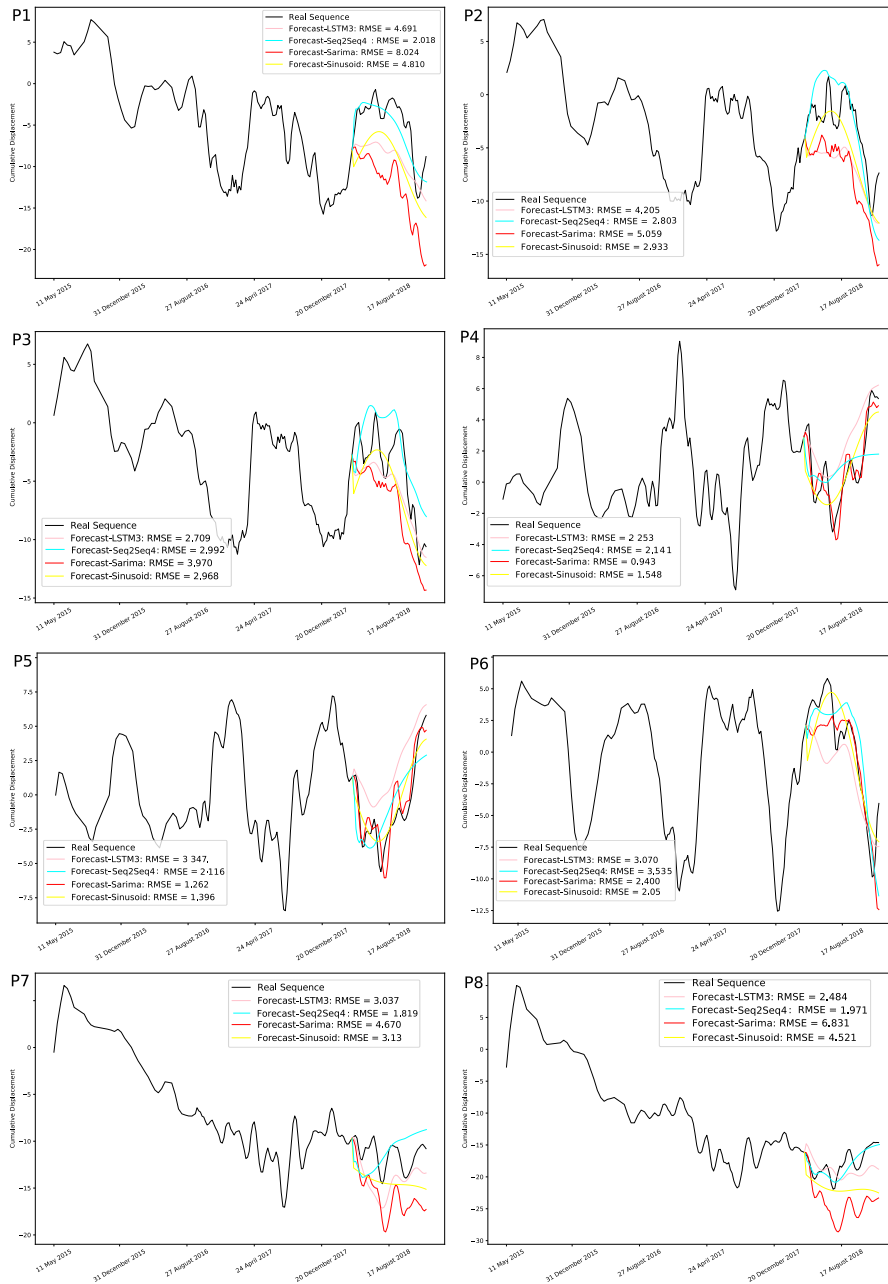


Figure 8. InSAR example forecasts of eight sample signals: LSTMs, SARIMA and Sinusoid Fitting. $N_y = 9$ months ($N_x = 9$ months for LSTMs). The top six signals are highly seasonal signals whereas the bottom two are highly un-seasonal

353

5.2 Randomly Selected Signals

354

355

356

357

358

359

360

361

Finally, we select 2000 points at random from the Normanton dataset with no regard to seasonality and test the methods that performed best on the seasonal signals: SARIMA and Seq2Seq4. We no longer consider LSTM3 since it was trained specifically on highly seasonal signals. Points P7-P8 shown in Figure 8 illustrate the challenges of time-series prediction for non-seasonal signals. Figure 7 shows that the relative variation in RMSE with prediction window is similar to that for seasonal signals. However, this figure shows that none of the methods perform better than the constant value prediction when signals are randomly selected (see also Supp. Figure 5).

362

363

364

365

366

367

368

369

370

371

372

373

Figure 9 shows the relationship between forecast performance (RMSE) and seasonality ($SIndex_{ACF}$) for a prediction window of 9 months for the Seq2Seq4, SARIMA and Sinu Methods. For Seq2Seq4, the forecast performance appears independent of seasonality, whereas the SARIMA and Sinu methods perform better (decreased RMSE) with increased seasonality. To test the statistical significance of this relationship, we set the null hypothesis (H_0) that the slope of the regression line is zero and the test hypothesis (H_1) that the slope of the regression line is negative. The p-values of the standard linearity test are 0.0014 ; 7.6×10^{24} and 3.9×10^{31} for Seq2Seq4, SARIMA and Sinu respectively. These values all exceed a significance threshold of 0.001 . There is a clearly statistically significant decrease in RMSE with an increase of $SIndex_{ACF}$ for SARIMA and Sinu, while the relationship is close to the significant limit for Seq2Seq4. A similar pattern is seen for all prediction windows (Supp. Figure 6).

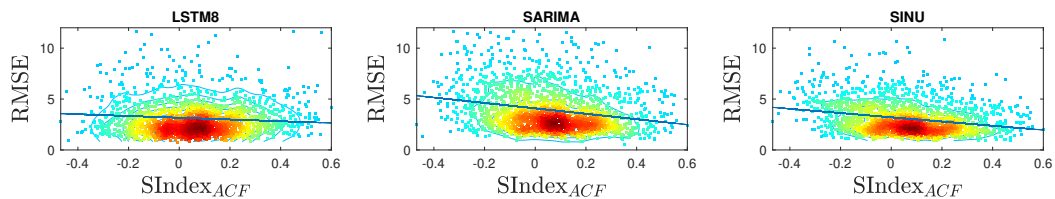


Figure 9. RMSE vs Seasonality Seq2Seq4, SARIMA and Sinu Methods. Plots show are for prediction windows of 9 months, with full results for predictions windows of 1-9 months shown in Supp Figure 6.

374

6 Discussion

375

376

377

378

379

380

381

Previous studies have reported annual variations in InSAR data associated with processes such as tropospheric water vapour (Heleno et al., 2010), thermal contraction and expansion (Lazecky et al., 2016), ground water (Bell et al., 2008) and freeze-thaw cycles (Daout et al., 2017). We find that our dataset from the Normanton area of the United Kingdom also contains signals with periodic variations, the strongest of which are clustered on large warehouses suggesting the dominant effect here is thermal expansion and contraction of man-made structures.

382

383

384

385

386

387

388

389

We test the ability of a range of established time series prediction methods to forecast InSAR time series and find that several methods perform better than a constant value prediction when signals dominated by periodic variations are considered. The lowest RMSE values are obtained for SARIMA when considering short term predictions (<3 months), whereas sinusoid extrapolation performs best for longer predictions (>6 months). However, for non-seasonal signals, the simple extrapolation of a constant function perform better overall than any of the more sophisticated time series prediction methods. Comparisons between seasonality and RMSE show a statistically significant improvement

390 in performance with increasing seasonality, which suggests pre-processing should be used
 391 to select appropriate points before time-series prediction is applied.

392 The metrics used only compare the global distribution of RMSE values, but the
 393 breadth of the distribution and scatter of outliers shows that the misfit is highly vari-
 394 able between observation points, even when seasonality is taken into account. Thus, if
 395 a prediction for a single observation point is required, there may be a large misfit in the
 396 prediction even for the best performing approaches, but a poorly performing method might
 397 produce a very accurate prediction.

398 The machine learning methods (LSTM and Seq2Seq) tested performed well in some
 399 cases, with the use of multivariate or concatenated signals improving the performance.
 400 However, it is interesting that they performed less well overall than simple extrapola-
 401 tion of a constant value (for non-seasonal signals) or a sinusoid (for seasonal signals). In-
 402 terestingly, the performance of the machine learning methods only improved slightly with
 403 increasing seasonality, suggesting that they are failing to capture the periodic compo-
 404 nent of the signal, perhaps because they are only trained over 9 months. Poor perfor-
 405 mance in predicting financial time series using LSTMs has also been reported (Sirignano
 406 & Cont, 2019). This is assumed to be related to the non-stationary nature of the data
 407 and the inability of LSTMs to model feedback effectively. Improvements in prediction
 408 using LSTMs should follow through both large increases in training data (number of data
 409 sequences and length of sequences) together with the integration of SARIMA type feed-
 410 back modelling.

411 In this study, we have focused on predictions for windows of less than the period
 412 of the signal (1 year), but both SARIMA and sinusoid extrapolation are able to predict
 413 for an arbitrary amount of time into the future. Figure 10 demonstrates that predictions
 414 for several years into the future show plausible time series, but unfortunately, no quan-
 415 titative evaluation is possible until a longer dataset of measurements is acquired. Sim-
 416 ilarly, LSTM methods require a training window that is at least as long as the predic-
 417 tion window, and will require longer timeseries before long-term predictions can be tested.

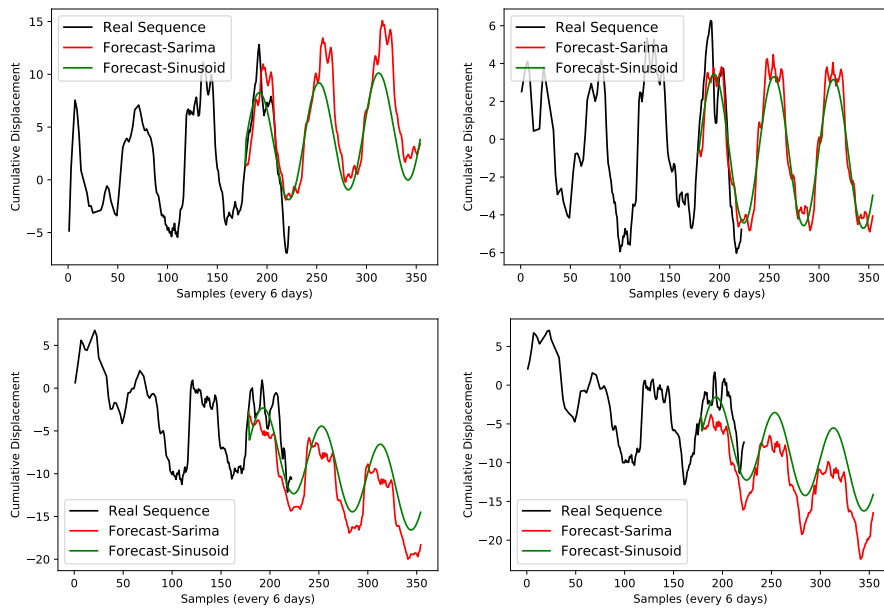


Figure 10. InSAR example forecasts of seasonal signals (far into the future: 3 years)

418 Real-time monitoring and ground motion forecasting of periodic signals from InSAR data
 419 could be used in one of two ways. The first of these is to predict seasonally varying ground
 420 motion signals that could otherwise obscure subtle deformation changes that could be
 421 pre-cursors to rapid and critical collapses (Selvakumaran et al., 2018). In this case, the
 422 reduction in background noise could enable the detection of anomalous or unexpected
 423 behaviour. Alternatively, the periodic motion itself is of interest to insurance companies
 424 looking to forecast claims due to ground cracking and subsidence (Crilly, 2001), or bridge
 425 motion (Lazecky et al., 2016). The broad distribution of misfit values suggests these ap-
 426 proaches will only be useful when considering the distribution of a large number of dat-
 427 apoints, and the probability of a good prediction for any single observation point is quite
 428 small.

429 This is a proof-of-concept study and the methods described here can be further re-
 430 fined. Possible future directions include testing different neural network architectures in-
 431 cluding convolutional LSTMs and attention based systems; the combination of SARIMA
 432 and LSTMs; the integration of spatial analysis using CNNs and multivariate prediction
 433 using Vector Autoregression. Future developments in machine learning and artificial in-
 434 telligence may improve performance, but the lack of periodic or repeating signals within
 435 the dataset may always be a barrier to time series prediction.

436 7 Conclusion

437 In this proof-of-concept study, we have tested a range of time series prediction tools on
 438 ground motion data collected using InSAR. For randomly-selected data, a simple con-
 439 stant value prediction outperforms both conventional time series analysis and forecast-
 440 ing methods such as SARIMA and supervised machine learning approaches such as LSTMs.
 441 This reflects the stochastic nature of the signals and the difficulties in using any trained
 442 system to predict far into the future. The time series prediction methods performed bet-
 443 ter on signals containing strong annual variations, and both LSTM based architectures
 444 and SARIMA performed better over short periods of time (less than three months) than
 445 the extrapolation of a sinusoidal function. This suggests that a pre-processing step could
 446 be used to select signals that are suitable for forecasting. However, further developments
 447 in machine learning and artificial intelligence will be needed before time series predic-
 448 tions of InSAR data are sufficiently reliable to be used in practice.

449 8 Acknowledgements

450 We thank SatSense Ltd for access to their dataset over the Normanton/Castleford
 451 area. This work was funded by the Digital Environment Programme under NE/S016104/1.

452 References

- 453 Aldiss, D., Burke, H., Chacksfield, B., Bingley, R., Teferle, N., Williams, S., . . .
 454 Press, N. (2014). Geological interpretation of current subsidence and uplift
 455 in the london area, uk, as shown by high precision satellite-based surveying.
 456 *Proceedings of the Geologists' Association*, 125(1), 1–13.
- 457 Anantrasirichai, N., Biggs, J., Albino, F., & Bull, D. (2019a). The application of
 458 convolutional neural networks to detect slow, sustained deformation in insar
 459 time series. *Geophysical Research Letters*, 46(21), 11850–11858.
- 460 Anantrasirichai, N., Biggs, J., Albino, F., & Bull, D. (2019b). A deep learning ap-
 461 proach to detecting volcano deformation from satellite imagery using synthetic
 462 datasets. *Remote Sensing of Environment*, 230, 111179.
- 463 Anantrasirichai, N., Biggs, J., Albino, F., Hill, P., & Bull, D. (2018). Applica-
 464 tion of machine learning to classification of volcanic deformation in routinely
 465 generated insar data. *Journal of Geophysical Research: Solid Earth*, 123(8),

- 466 6592–6606.
- 467 Banks, D., Davies, C., & Davies, W. (1995). The Chalk as a karstic aquifer: evi-
468 dence from a tracer test at Stanford Dingley, Berkshire, UK. *Quarterly Journal*
469 *of Engineering Geology and Hydrogeology*, 28(Supplement 1), S31–S38.
- 470 Bell, J. W., Amelung, F., Ferretti, A., Bianchi, M., & Novali, F. (2008). Perma-
471 nent scatterer insar reveals seasonal and long-term aquifer-system response
472 to groundwater pumping and artificial recharge. *Water Resources Research*,
473 44(2).
- 474 Box, G. E., Jenkins, G. M., Reinsel, G. C., & Ljung, G. M. (2015). *Time series*
475 *analysis: forecasting and control*. John Wiley & Sons.
- 476 Brockwell, P. J., & Davis, R. A. (2016). *Introduction to time series and forecasting*.
477 springer.
- 478 Burke, H., Hough, E., Morgan, D., Hughes, L., & Lawrence, D. (2015). Approaches
479 to inform redevelopment of brownfield sites: An example from the Leeds area
480 of the West Yorkshire coalfield, UK. *Land Use Policy*, 47, 21–331.
- 481 Carla, T., Intrieri, E., Di Traglia, F., & Casagli, N. (2016). A statistical-based
482 approach for determining the intensity of unrest phases at stromboli volcano
483 (southern italy) using one-step-ahead forecasts of displacement time series.
484 *Natural Hazards*, 84(1), 669–683.
- 485 Chambers, J., Weller, A., Gunn, D., Kuras, O., Wilkinson, P., Meldrum, P., . . . oth-
486 ers (2008). Geophysical anatomy of the hollin hill landslide, north yorkshire,
487 uk. In *Near surface 2008-14th eage european meeting of environmental and*
488 *engineering geophysics* (pp. cp–64).
- 489 Chen, J., & Boccelli, D. L. (2018). Forecasting hourly water demands with seasonal
490 autoregressive models for real-time application. *Water Resources Research*,
491 54(2), 879–894.
- 492 Cho, K., Van Merriënboer, B., Gulcehre, C., Bahdanau, D., Bougares, F., Schwenk,
493 H., & Bengio, Y. (2014). Learning phrase representations using rnn encoder-
494 decoder for statistical machine translation. *arXiv preprint arXiv:1406.1078*.
- 495 Cleveland, R. B., Cleveland, W. S., McRae, J. E., & Terpenning, I. (1990). Stl: a
496 seasonal-trend decomposition. *Journal of official statistics*, 6(1), 3–73.
- 497 Cleveland, W. S. (1979). Robust locally weighted regression and smoothing scatter-
498 plots. *Journal of the American statistical association*, 74(368), 829–836.
- 499 Colesanti, C., Ferretti, A., Novali, F., Prati, C., & Rocca, F. (2003). Sar monitoring
500 of progressive and seasonal ground deformation using the permanent scatterers
501 technique. *IEEE Transactions on Geoscience and Remote Sensing*, 41(7),
502 1685–1701.
- 503 Crilly, M. (2001). Analysis of a database of subsidence damage. *Structural survey*,
504 19(1), 7–15.
- 505 Daout, S., Doin, M.-P., Peltzer, G., Socquet, A., & Lasserre, C. (2017). Large-scale
506 insar monitoring of permafrost freeze-thaw cycles on the tibetan plateau. *Geo-*
507 *physical Research Letters*, 44(2), 901–909.
- 508 Gaddes, M., Hooper, A., & Bagnardi, M. (2019). Using machine learning to auto-
509 matically detect volcanic unrest in a time series of interferograms. *Journal of*
510 *Geophysical Research: Solid Earth*.
- 511 Greff, K., Srivastava, R. K., Koutník, J., Steunebrink, B. R., & Schmidhuber, J.
512 (2017, Oct). Lstm: A search space odyssey. *IEEE Transactions on Neural*
513 *Networks and Learning Systems*, 28(10), 2222–2232.
- 514 Hamilton, J. D. (1994). *Time series analysis* (Vol. 2). Princeton New Jersey.
- 515 Hartmann, D. L., Michelsen, M. L., & Klein, S. A. (1992). Seasonal variations
516 of tropical intraseasonal oscillations: A 20–25-day oscillation in the western
517 pacific. *Journal of the atmospheric sciences*, 49(14), 1277–1289.
- 518 Heleno, S. I., Frischknecht, C., d’Oreye, N., Lima, J., Faria, B., Wall, R., & Kervyn,
519 F. (2010). Seasonal tropospheric influence on sar interferograms near the
520 itcz—the case of fogo volcano and mount cameroon. *Journal of African Earth*

- 521 *Sciences*, 58(5), 833–856.
- 522 Hochreiter, S., & Schmidhuber, J. (1997). Long short-term memory. *Neural Compu-*
523 *tation*, 9(8), 1735–1780.
- 524 Hylleberg, S. (1995). Tests for seasonal unit roots general to specific or specific to
525 general? *Journal of Econometrics*, 69(1), 5–25.
- 526 Hyndman, R. J., Khandakar, Y., et al. (2007). *Automatic time series for forecasting:*
527 *the forecast package for r* (No. 6/07).
- 528 Kingma, D.-P., & Ba, J. (2015). Adam: A Method for Stochastic Optimization. *In-*
529 *ternational Conference on Learning Representations (ICLR)*.
- 530 Lake, R., Northmore, K., Dean, M., & Tragheim, D. (1992). Leeds: a geological
531 background for planning and development: 1: 10000 sheets SE23NW, NE, SE
532 and SE33NW, NE, SW, SE: parts of 1: 50000 geological sheets 69 (Bradford),
533 70 (Leeds), 77 (Huddersfield) and 78 (Wakefield).
- 534 Lamont-Black, J., Younger, P. L., Forth, R. A., Cooper, A. H., & Boniface, J. P.
535 (2002). A decision-logic framework for investigating subsidence problems po-
536 tentially attributable to gypsum karstification. *Engineering geology*, 65(2-3),
537 205–215.
- 538 Lazecky, M., Hlavacova, I., Bakon, M., Sousa, J. J., Perissin, D., & Patricio, G.
539 (2016). Bridge displacements monitoring using space-borne x-band sar inter-
540 ferometry. *IEEE Journal of Selected Topics in Applied Earth Observations and*
541 *Remote Sensing*, 10(1), 205–210.
- 542 Mazzanti, P., Rocca, A., Bozzano, F., Cossu, R., & Floris, M. (n.d.). Landslides
543 forecasting analysis by displacement time series derived from satellite insar
544 data: preliminary results. *Small*, 5000, 50–000.
- 545 McCay, A. T., Valyrakis, M., & Younger, P. L. (2018). A meta-analysis of coal
546 mining induced subsidence data and implications for their use in the carbon
547 industry. *International Journal of Coal Geology*, 192, 91–101.
- 548 Milillo, P., Giardina, G., DeJong, M., Perissin, D., & Milillo, G. (2018). Multi-
549 temporal insar structural damage assessment: The london crossrail case study.
550 *Remote Sensing*, 10(2), 287.
- 551 Rebane, J., Karlsson, I., Denic, S., & Papapetrou, P. (2018). Seq2seq rnns and arima
552 models for cryptocurrency prediction: A comparative study. *SIGKDD Fintech*,
553 18.
- 554 Rumelhart, D. E., Hinton, G. E., & Williams, R. J. (1986, October). Learning repre-
555 sentations by back-propagating errors. *Nature*, 323, 533–.
- 556 Selvakumaran, S., Plank, S., Geiß, C., Rossi, C., & Middleton, C. (2018). Remote
557 monitoring to predict bridge scour failure using interferometric synthetic aper-
558 ture radar (insar) stacking techniques. *International journal of applied earth*
559 *observation and geoinformation*, 73, 463–470.
- 560 Sirignano, J., & Cont, R. (2019). Universal features of price formation in financial
561 markets: perspectives from deep learning. *Quantitative Finance*, 19(9), 1449–
562 1459.
- 563 Spaans, K., & Hooper, A. (2016). Insar processing for volcano monitoring and other
564 near-real time applications. *Journal of Geophysical Research: Solid Earth*,
565 121(4), 2947–2960.
- 566 Sutskever, I., Vinyals, O., & Le, Q. (2014). Sequence to sequence learning with neu-
567 ral networks. *Advances in NIPS*.
- 568 Torres, D. G., & Qiu, H. (2018). *Applying recurrent neural networks for multivariate*
569 *time series forecasting of volatile financial data*. Stockholm: KTH Royal Insti-
570 tute of Technology.
- 571 Valade, S., Ley, A., Massimetti, F., D’Hondt, O., Laiolo, M., Coppola, D., . . . Wal-
572 ter, T. R. (2019). Towards global volcano monitoring using multisensor
573 sentinel missions and artificial intelligence: The mounts monitoring system.
574 *Remote Sensing*, 11(13), 1528.
- 575 Watson, K. M., Bock, Y., & Sandwell, D. T. (2002). Satellite interferometric ob-

576 servations of displacements associated with seasonal groundwater in the los
577 angeles basin. *Journal of Geophysical Research: Solid Earth*, 107(B4).
578 Zubaidi, S. L., Dooley, J., Alkhaddar, R. M., Abdellatif, M., Al-Bugharbee, H., &
579 Ortega-Martorell, S. (2018). A novel approach for predicting monthly wa-
580 ter demand by combining singular spectrum analysis with neural networks.
581 *Journal of hydrology*, 561, 136–145.